Spatial-Aliasing-Free Radiation Synthesis using Infinite Line Source Arrays

This manuscript is compiled from the LaTeX code that was used to submit the PDF-version of the peer-reviewed paper
Schultz, F.; Rettberg, T.; Spors. S. (2014): "On Spatial-Aliasing-Free Sound Field Reproduction using Infinite Line Source Arrays."
In: *Proc. of the 136th Audio Eng. Soc. Conv., Berlin*, #9078. to the Audio Engineering Society.
The present tutorial includes enhanced calculus, explanations for didactical purpose and further clarification as well as errata.
pdfTeX, amsmath, amssymb, TikZ, IEEEtran.cls, conference, US letter is used for typesetting.

Frank Schultz, Till Rettberg and Sascha Spors
Institute of Communications Engineering, University of Rostock
R.-Wagner-Str. 31 (Haus 8), D-18119 Rostock, Germany
{frank.schultz, till.rettberg, sascha.spors}@uni-rostock.de
http://spatialaudio.net

***Keywords*—Sound Reinforcement, Line Source Array, Wavefront Sculpture Technology, Waveguide, Sound Field Synthesis, Spatial Aliasing.**

***Abstract*—Concert sound reinforcement systems aim at the reproduction of homogeneous sound fields over extended audiences for the whole audio bandwidth. For the last two decades this has been mostly approached by using so called line source arrays due to their superior ability to produce homogeneous sound fields. Design and setup criteria for line source arrays were derived as Wavefront Sculpture Technology in literature. This paper introduces a viewpoint on the problem at hand by utilizing a signal processing model that was developed for sound field synthesis. It will be shown that the optimal radiation of a line source array can be considered as a special case of spatial-aliasing-free synthesis of a wave front that propagates perpendicular to the array. For high frequencies the so called waveguide operates as a spatial lowpass filter and therefore attenuates energy that otherwise would lead to spatial aliasing artifacts.**

I. Introduction

Wavefront Sculpture Technology[1] (WST) and its derived criteria [1]–[3] represent the modern fundamentals of *line source array* (LSA) radiation. Similar findings were also discussed in [4]. The WST criteria define how to engineer LSA elements (single loudspeaker cabinets) and how to setup an LSA in order to reproduce homogeneous sound fields over a large audience area. The WST criteria 1-3 [3, pg. 929] define how the LSA elements have to be designed arranging an in-phase driven, straight LSA of finite length. For high frequencies (>1-2 kHz) the criteria suggest to use line pistons with specific length and infinitesimal width as individual sources. This will be achieved by waveguides that are able to "generate a flat, isophasic" wavefront [3, pg. 916]. This feature constitutes the main difference to a *line array* for which regular (horn-loaded) loudspeakers are vertically stacked. Typically the latter produce undesired interference patterns – which we will term spatial aliasing – that corrupt the desired sound field mainly at high frequencies. LSA designs aim at avoiding this. The WST criterion 4 defines an optimal array curvature to provide a homogeneous and frequency independent amplitude decay over the audience distance. The WST criterion 5 interrelates the length of the waveguide and a maximum possible splaying angle between the LSA elements.

Model- or data based loudspeaker directivities have been taken into account for the prediction of sound fields generated by LSAs [5]–[9]. Radiation synthesis has been approached by solving an inverse problem using numerical optimization and driving the LSA elements with finite impulse response (FIR) filters [10]–[14].

In this paper we approach the radiation synthesis problem analytically, by applying findings from the broader theory of sound field synthesis (SFS). In fact the present work is strongly related to the discussions in [15]. Linear loudspeaker arrays have been discussed for *Wave Field Synthesis* (WFS) [16] and for the *Spectral Division Method* (SDM) [17]. Usually, the individual sources – termed *secondary sources* in SFS – are modeled as spherical monopoles, resulting in a simplified mathematical formulation. Approaches exist which implement model- or data based loudspeaker directivities into SFS algorithms [18]–[23].

We briefly revisit SFS theory and derive a suitable driving function for an LSA beginning with a continuous *secondary source distribution* (SSD). For clarity of analysis, spatial discretization [1, II.3.] and spatial truncation [24] of the LSA are treated separately. This paper's scope is restricted to the spatial sampling process and its implications. We propose an optimal waveguide design from a theoretical viewpoint which is in agreement with the known WST criteria 1,2. We will show that an ideal waveguide has a directivity that theoretically is able to suppress all spatial-aliasing components for uniformly driven LSAs. The simulations are compared to measurements of a real waveguide. Spatial truncation and its interaction with discretization are discussed subsequently in [25].

II. NOMENCLATURE

This section defines conventions and notations that are used throughout this study. Linear acoustics with constant speed of sound $c = 343\,\mathrm{m/s}$ in a dissipationless medium under free-field

[1]Wavefront Sculpture Technology® is a registered trademark of L-ACOUSTICS US, LLC. We omit the labeling in the remainder of the paper and will only use the relevant research results.

conditions is assumed. A position vector in space

$$\mathbf{x} = \begin{pmatrix} x \\ y \\ z \end{pmatrix} = \|\mathbf{x}\| \cdot \begin{pmatrix} \cos\varphi & \sin\vartheta \\ \sin\varphi & \sin\vartheta \\ & \cos\vartheta \end{pmatrix} \tag{1}$$

is defined with azimuth $\varphi \in [0, 2\,\pi)$, colatitude $\vartheta \in [0, \pi]$ and the vector norm $\|\mathbf{x}\| = r = \sqrt{x^2 + y^2 + z^2}$. The wave number vector is given by

$$\mathbf{k} = \begin{pmatrix} k_x \\ k_y \\ k_z \end{pmatrix} = \left(\frac{\omega}{c}\right) \cdot \begin{pmatrix} \cos\varphi & \sin\vartheta \\ \sin\varphi & \sin\vartheta \\ & \cos\vartheta \end{pmatrix}, \tag{2}$$

with $\frac{\omega}{c} = \sqrt{\langle \mathbf{k}, \mathbf{k} \rangle}$, denoting the scalar product with $\langle \cdot, \cdot \rangle$. The dispersion relation of linear acoustics

$$\left(\frac{\omega}{c}\right)^2 = k_x^2 + k_y^2 + k_z^2 \tag{3}$$

holds. The scalar product $\langle \mathbf{k}, \mathbf{x} \rangle = k_x\, x + k_y\, y + k_z\, z$ is used for the description of plane waves in cartesian coordinates.

The temporal angular frequency $\omega = 2\,\pi\, f$ in rad/s is linked to the temporal frequency f in Hz. The imaginary number is denoted by j ($\mathrm{j}^2 = -1$). The temporal Fourier transform sign and normalization convention

$$p(\mathbf{x}, t) = \frac{1}{2\,\pi} \int_{-\infty}^{+\infty} P(\mathbf{x}, \omega)\, \mathrm{e}^{+\mathrm{j}\,\omega\, t} \mathrm{d}\omega, \tag{4}$$

$$P(\mathbf{x}, \omega) = \int_{-\infty}^{+\infty} p(\mathbf{x}, t)\, \mathrm{e}^{-\mathrm{j}\,\omega\, t} \mathrm{d}t \tag{5}$$

is used for the relationship of the sound pressure $p(\mathbf{x}. t)$ in time domain and its temporal spectrum $P(\mathbf{x}, \omega)$. The spatial Fourier transform sign and normalization convention

$$P(x, y, z, \omega) = \frac{1}{2\,\pi} \int_{-\infty}^{+\infty} P(x, k_y, z, \omega)\, \mathrm{e}^{-\mathrm{j}\, k_y\, y} \mathrm{d}k_y, \tag{6}$$

$$P(x, k_y, z, \omega) = \int_{-\infty}^{+\infty} P(x, y, z, \omega)\, \mathrm{e}^{+\mathrm{j}\, k_y\, y} \mathrm{d}y \tag{7}$$

is used. A spectrum with respect to time and space $P(k_y, \omega)$ is termed spatio-temporal spectrum and due to its nature of a plane wave decomposition using the spatial Fourier transform, the term angular spectrum is used in the remainder. The conventions imply that the wave vector $\mathbf{k}$ denotes the propagation direction of the wave. Thus,

$$p(\mathbf{x}, t) = \Re\left\{ \mathrm{e}^{-\mathrm{j}\,\langle \mathbf{k}_{\mathrm{PW}}, \mathbf{x} \rangle}\, \mathrm{e}^{+\mathrm{j}\,\omega_{\mathrm{PW}}\, t} \right\} \tag{8}$$

describes a unit amplitude monochromatic plane wave which propagates into direction of $\mathbf{k}_{\mathrm{PW}} = (k_{x,\mathrm{PW}},\, k_{y,\mathrm{PW}},\, k_{z,\mathrm{PW}})^T$ and oscillates with ω_{PW}. $\Re\{\cdot\}$ denotes the real part.

For the chosen conventions the three-dimensional, freefield Green's function is defined by

$$G(\|\mathbf{x} - \mathbf{x_0}\|, \omega) = \frac{\mathrm{e}^{-\mathrm{j}\,\frac{\omega}{c}\,\|\mathbf{x} - \mathbf{x_0}\|}}{4\,\pi\,\|\mathbf{x} - \mathbf{x_0}\|} \tag{9}$$

with the source position $\mathbf{x_0}$ [26, Ch. 27]. It models an ideal, radiating spherical monopole [27, Ch. 5.16].

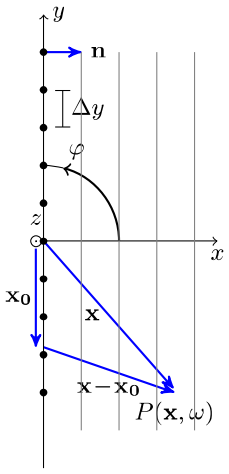

Fig. 1: Side view of the discussed SSD setup. The infinite SSD is located on the y-axis. Sound field reproduction is considered within the xy-plane ($x > 0$). The SSD becomes continuous for a secondary source spacing $\Delta y \to 0$. The LSA is later modeled by spatially sampling the driving function and modifying the Green's function in (23) to account for piston-like sources.

The SSD, i.e. the loudspeaker array with infinite length and spatial discretization Δy is located on the y-axis. The sound field is evaluated in the xy-plane for $x > 0$, cf. Fig. 1.

III. Sound Field Synthesis

A well known approach for numerical sound field prediction of a finite LSA [9] is based on the complex summation of N LSA elements, that are defined by their individual and frequency dependent farfield directivity patterns $A_n(\varphi, \vartheta, \omega)$ and temporal frequency dependent weightings $D(\mathbf{x_{0,n}}, \omega)$. This temporal frequency filters define magnitude, phase and delay for the individual secondary sources and are termed *driving functions* in SFS. For discrete source positions $\mathbf{x_{0,n}}$ we can therefore write, cf. [9, (11)], [28, (2)]

$$P(\mathbf{x}, \omega) = \sum_{n=1}^{N} D(\mathbf{x_{0,n}}, \omega)\, A_n(\mathbf{x}, \mathbf{x_{0,n}}, \omega)\, \frac{\mathrm{e}^{-\mathrm{j}\,\frac{\omega}{c}\,\|\mathbf{x} - \mathbf{x_{0,n}}\|}}{4\,\pi\,\|\mathbf{x} - \mathbf{x_{0,n}}\|}. \tag{10}$$

While this equation is useful for the prediction of sound fields and constitutes the basis for numerical optimization schemes [10]–[14], it does not explicitly reveal how spatial aliasing and undesired side lobes are generated and where to find their physical origin. Since we are majorly interested in this question, the problem is retraced to the fundamentals of sound field synthesis. The Rayleigh integral using Neumann Green's function [29] is subsequently extended towards a full signal processing framework cf. Fig. 2, that was developed for SFS using planar and linear arrays, cf. [30, Ch. 5], [15], [31]–[35]. In [30, Ch. 5], [15] WFS-based reproduction of a virtual spherical monopole was analyzed with the acoustic signal processing framework. This signal processing model will be used throughout the paper for uniformly driven, infinite linear arrays, whereas a subsequent study [25] discusses uniformly driven, finite length linear arrays. The analysis performed here can be considered as a special case of SFS.

A. 3D SFS with a continuous SSD

We start our discussion with the fundamentals of SFS, cf. [29], [36], [37]. First, consider a planar SSD within the yz-plane for which we introduce the position vector $\mathbf{x_0} = (0, y_0, z_0)^T$ on the SSD. SFS in the target half-space $x > 0$, i.e. for $\mathbf{x} = (x > 0, y, z)^T$ is realized by the so called single layer potential (SLP) [29]

$$P(\mathbf{x}, \omega) = \iint_{-\infty}^{+\infty} D(\mathbf{x_0}, \omega)\, G(\|\mathbf{x} - \mathbf{x_0}\|, \omega)\, \mathrm{d}y_0\, \mathrm{d}z_0. \tag{11}$$

This approach is known as three-dimensional SFS.

The implicit solution of the driving function is well known. It corresponds to the Rayleigh integral under Neumann boundary condition imposed to the Green's function [29]. The driving function reads

$$\begin{aligned} D(\mathbf{x_0}, \omega) &= -2\, \frac{\partial P(\mathbf{x_0}, \omega)}{\partial n} \\ &= -2\, \langle \operatorname{grad}_{\mathbf{x}} P(\mathbf{x}, \omega)\big|_{\mathbf{x}=\mathbf{x_0}}\, ,\, \mathbf{n}(\mathbf{x_0}) \rangle, \end{aligned} \tag{12}$$

using the directional derivative with the unit inward normal vector $\mathbf{n}(\mathbf{x_0}) = (1, 0, 0)^T$. Provided that the sound pressure $P(\mathbf{x}, \omega)$ of a virtual source is known and assuming that the integral (11) converges, the solution for $P(\mathbf{x}, \omega)$ is unique and exact, as expected for the Rayleigh integral as a forward wave field propagator [38, Ch. 6.5, 9]. This approach was used for the modern[2] formulation of 3D Wave Field Synthesis [16], [41].

An explicit solution of the driving function is derived by applying the convolution theorem to the integral (11). For uniform SSD characteristics, the free-field Green's function is shift-invariant and (23) can be interpreted as the convolution

$$P(\mathbf{x}, \omega) = D(\mathbf{x}, \omega)\ *_y *_z\, G(\mathbf{x}, \mathbf{0}, \omega) \tag{13}$$

along y and z for a chosen x in the target half-space. The Green's function $G(\mathbf{x}, \mathbf{0}, \omega)$ in the origin $\mathbf{x_0} = \mathbf{0}$ is used as the reference monopole and is convolved with the driving function, cf. upper row of Fig. 2. The convolution corresponds a multiplication in the angular spectrum domain

$$P(x, k_y, k_z, \omega) = D(x, k_y, k_z, \omega) \cdot G_0(x, k_y, k_z, \omega), \tag{14}$$

for which (7) has to be applied w.r.t. $y \circ\!\!-\!\!\bullet\, k_y$ and $z \circ\!\!-\!\!\bullet\, k_z$. Explicitly solving for $D(x, k_y, k_z, \omega)$ yields

$$D(x, k_y, k_z, \omega) = \frac{P(x, k_y, k_z, \omega)}{G_0(x, k_y, k_z, \omega)}, \tag{15}$$

and the inverse spatial Fourier transform (6) leads to the driving function

$$D(\mathbf{x_0}, \omega) = \frac{1}{4\,\pi^2} \iint_{-\infty}^{+\infty} \frac{P(x, k_y, k_z, \omega)}{G_0(x, k_y, k_z, \omega)}\, \mathrm{e}^{-\mathrm{j}(k_y y_0 + k_z z_0)}\, \mathrm{d}k_y\, \mathrm{d}k_z, \tag{16}$$

provided that the integral converges. This technique as an explicit SFS solution was introduced as Spectral Division Method (SDM) in literature [42], [17, p. 2040]. The angular spectrum of the desired sound field is given as

$$P(x, k_y, k_z, \omega) = \check{P}(k_y, k_z, \omega)\, \mathrm{e}^{-\mathrm{j}\, k_x\, x}\, 2\,\pi\, \delta(\omega - \omega_{\mathrm{PW}}). \tag{17}$$

It can be shown that the driving function is independent from the chosen spatial position x [17], [29]. The driving function (16) can therefore reformulated to

$$D(\mathbf{x_0}, \omega) = \frac{1}{4\,\pi^2} \iint_{-\infty}^{+\infty} \frac{\check{P}(k_y, k_z, \omega)}{-\mathrm{j}\,\frac{1}{2\,k_x}}\, \mathrm{e}^{-\mathrm{j}(k_y y_0 + k_z z_0)}\, \mathrm{d}k_y\, \mathrm{d}k_z, \tag{18}$$

for which

$$k_x = \begin{cases} +\sqrt{(\frac{\omega}{c})^2 - (k_y^2 + k_z^2)} & \text{for } (\frac{\omega}{c})^2 > (k_y^2 + k_z^2) \\ -\mathrm{j}\,\sqrt{(k_y^2 + k_z^2) - (\frac{\omega}{c})^2} & \text{for } (k_y^2 + k_z^2) > (\frac{\omega}{c})^2 \end{cases} \tag{19}$$

holds for the region of interest, cf. [38, Ch. 2.2], [43, Ch. 2.6]. The 1st case in (19) describes propagating waves, the 2nd case corresponds to evanescent waves.

The monochromatic plane wave (8) with radiation direction $\mathbf{k}_{\mathrm{PW}} = (k_{x,\mathrm{PW}},\, k_{y,\mathrm{PW}},\, k_{z,\mathrm{PW}})^T$ into the target half-space

$$p(\mathbf{x}, t) = \mathrm{e}^{-\mathrm{j}\,\langle \mathbf{k}_{\mathrm{PW}}, \mathbf{x} \rangle}\, \mathrm{e}^{+\mathrm{j}\,\omega_{\mathrm{PW}}\, t} \tag{20}$$

is decomposed into [17, (49)], [44, (C.6)]

$$P(x, k_y, k_z, \omega) = \mathrm{e}^{-\mathrm{j}\, k_{x,\mathrm{PW}} \cdot x} \times \overbrace{4\,\pi^2\, \delta(k_y - k_{y,\mathrm{PW}})\ \delta(k_z - k_{z,\mathrm{PW}}) \cdot 2\,\pi\, \delta(\omega - \omega_{\mathrm{PW}})}^{\check{P}(k_y, k_z, \omega)}. \tag{21}$$

The driving function (18) is derived to [17, (7)], [44, (3.68)]

$$D(\mathbf{x_0}, \omega) = 2\,\mathrm{j}\, k_{x,\mathrm{PW}} \cdot \mathrm{e}^{-\mathrm{j}\, k_{y,\mathrm{PW}} \cdot y_0}\ \mathrm{e}^{-\mathrm{j}\, k_{z,\mathrm{PW}} \cdot z_0}\, 2\,\pi\, \delta(\omega - \omega_{\mathrm{PW}}), \tag{22}$$

which is also obtained by evaluating the directional derivative (12). This is due to the exact equivalence of WFS and SDM for 3D SFS [17], [29].

3D SFS with a planar, continuous SSD is not feasible for sound reinforcement and rather linear arrays were introduced. The fundamentals of so called 2.5D SFS using an infinite linear array are discussed in the next subsection, following [44, Ch. 3.7], [17, Sec. IIB]

B. 2.5D SFS with a continuous SSD

The sound field $P(\mathbf{x}, \omega)$ produced by an infinite, continuous, linear array is described similar to (11)

$$P(\mathbf{x}, \omega) = \int_{-\infty}^{+\infty} D(\mathbf{x_0}, \omega)\, G(\|\mathbf{x} - \mathbf{x_0}\|, \omega)\, \mathrm{d}y_0 \tag{23}$$

using $\mathbf{x} = (x > 0, y, z)^T$ and $\mathbf{x_0} = (0, y_0, 0)^T$ according to Fig. 1. The infinite linear SSD is incapable of radiating three dimensional plane waves due to the dimension reduction. Therefore the possible wave radiation directions correspond to a reduced set of wave number vectors, i.e. k_x, k_y and k_z cannot be controlled individually. The wave number k_y describes the wave propagation along the SSD orientation. The radial wave number k_r describes the radiation direction

[2] The term 'modern WFS' is frequently used for WFS that uses the Neumann Green's function Rayleigh integral, whereas 'traditional WFS' is referred to as the Dirichlet Green's function Rayleigh integral approach, e.g. [39], [40]

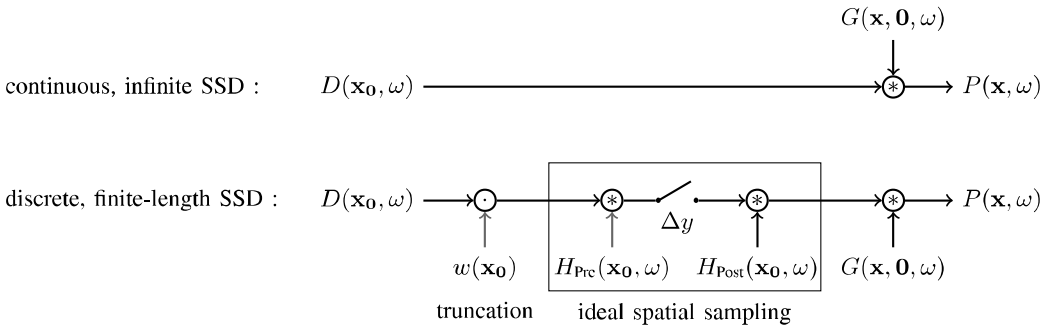

Fig. 2: The single layer potential for a linear SSD located on the y-axis. Representation of continuous, infinte-length case (top) and the discretized, finite-length model (bottom). Convolution is denoted by $\circledast$, multiplication by $\odot$.

of conical wavefronts. For a plane wave radiation direction $\vartheta_{\text{PW}}, \varphi_{\text{PW}}$

$$(\frac{\omega_{\text{PW}}}{c})^2 - k_{y,\text{PW}}^2 = \underbrace{(\frac{\omega_{\text{PW}}}{c})^2 \left(\cos^2 \varphi_{\text{PW}} \sin^2 \vartheta_{\text{PW}} + \cos^2 \vartheta_{\text{PW}}\right)}_{k_{r,\text{PW}}^2 = k_{x,\text{PW}}^2 + k_{z,\text{PW}}^2} \tag{24}$$

holds. For a desired ω_{PW} and chosen $k_{y,\text{PW}}$ [44, (3.76)]

$$(\frac{\omega_{\text{PW}}}{c})^2 - k_{y,\text{PW}}^2 = \text{const} = k_{r,\text{PW}}^2 \tag{25}$$

follows, and either ϑ_{PW} or φ_{PW} can be controlled.

Similar to (13) the convolution along the y-axis in (23) can be transferred to an angular spectrum multiplication w.r.t. k_y

$$P(x, k_y, z, \omega) = D(x, k_y, z, \omega) \cdot G_0(x, k_y, z, \omega). \tag{26}$$

This holds again under the assumption that the SSD characteristics is uniform, i.e. the Green's function is shift-invariant. Explicitly solving for $D(x, k_y, z, \omega)$ yields

$$D(x, k_y, z, \omega) = \frac{P(x, k_y, z, \omega)}{G_0(x, k_y, z, \omega)}, \tag{27}$$

and the inverse spatial Fourier transform (6) leads to the unknown driving function

$$D(\mathbf{x_0}. \omega) = \frac{1}{2\,\pi} \int_{-\infty}^{+\infty} \frac{P(x, k_y, z, \omega)}{G_0(x, k_y, z, \omega)}\, \mathrm{e}^{-\mathrm{j}\, k_y\, y_0}\, \mathrm{d}k_y, \tag{28}$$

provided that the integral converges.

We proceed with the derivation of a suitable driving function $D(y_0, \omega)$ and its angular spectrum $D(k_y, \omega)$ for a wave radiation perpendicular to the SSD, as this is considered a special case of SFS, which initially derived the first WST criteria [1].

C. Derivation of an LSA Driving Function for 2.5D SFS

A thorough derivation of the driving function is found in [44, Ch. 3.7], [17, II. B] and is briefly revisited here. First the angular spectrum for the Green's function $G(\mathbf{x}, \mathbf{0}, \omega)$ in the origin is given as [44, (C.10)], [17, (52)]

$$G_0(x, k_y, z, \omega) = -\frac{\mathrm{j}}{4}\, H_0^{(2)} \left(\sqrt{\left(\frac{\omega}{c}\right)^2 - k_y^2} \cdot \sqrt{x^2 + z^2} \right), \tag{29}$$

for $k_y^2 < (\frac{\omega}{c})^2$ (i.e. propagating waves), where $H_0^{(2)}(\cdot)$ denotes the 0^{th} order cylindrical Hankel function of 2^{nd} kind [45, §10.1]. For $k_y^2 > (\frac{\omega}{c})^2$ (i.e. evanescent waves)

$$G_0(x, k_y, z, \omega) = \frac{1}{2\,\pi}\, K_0 \left(\sqrt{k_y^2 - \left(\frac{\omega}{c}\right)^2} \cdot \sqrt{x^2 + z^2} \right) \tag{30}$$

holds, using the modified Bessel function $K_0(\cdot)$ of 0^{th} order of 2^{nd} kind [45, §10.1]. The angular spectrum of a desired plane wave into direction $\mathbf{k}_{\text{PW}} = (k_{x,\text{PW}},\, k_{y,\text{PW}},\, k_{z,\text{PW}})^T$ is given by

$$\begin{aligned} P(x, k_y, z, \omega) = {} & \mathrm{e}^{-\mathrm{j}\, k_{x,\text{PW}} \cdot x}\, \mathrm{e}^{-\mathrm{j}\, k_{z,\text{PW}} \cdot z} \times \\ & 2\,\pi\, \delta(k_y - k_{y,\text{PW}}) \cdot 2\,\pi\, \delta(\omega - \omega_{\text{PW}}) \end{aligned} \tag{31}$$

and with (28) follows [36, (3.74)], [17, (13)]

$$\begin{aligned} D(x, k_y, z, \omega) = {} & \frac{\mathrm{e}^{-\mathrm{j}\, k_{x,\text{PW}} \cdot x}\, \mathrm{e}^{-\mathrm{j}\, k_{z,\text{PW}} \cdot z}\, 2\,\pi\, \delta(\omega - \omega_{\text{PW}})}{-\frac{\mathrm{j}}{4}\, H_0^{(2)} \left(\sqrt{\left(\frac{\omega_{\text{PW}}}{c}\right)^2 - k_{y,\text{PW}}^2} \cdot \sqrt{x^2 + z^2} \right)} \times \\ & 2\,\pi\, \delta(k_y - k_{y,\text{PW}}) \end{aligned} \tag{32}$$

for propagating wave radiation. Note the application of the Delta function's sifting property. The numerator exhibits a three-dimensional problem (plane wave), while the denominator is two dimensional (linear array, cylindrical wave radiation). SFS, that employs this mismatch is known as 2.5D synthesis, for which the so called 2.5D Rayleigh integral was introduced in literature [30], [46]. Matching both geometries is conveniently realized, when we are only interested in the sound field within the xy-plane, i.e. $z = 0$ and thus consequently restrict the plane wave radiation only to this plane, i.e. $k_z = 0$. Hence, for $\vartheta_{\text{PW}} = \pi/2$ this yields an axial and radial wave number

$$k_{y,\text{PW}}^2 = (\frac{\omega_{\text{PW}}}{c}\, \sin \varphi_{\text{PW}})^2 \qquad k_{r,\text{PW}}^2 = (\frac{\omega_{\text{PW}}}{c}\, \cos \varphi_{\text{PW}})^2. \tag{33}$$

The driving functions's angular spectrum is then reformulated to [44, (3.78)], [17, (16)]

$$D(x, k_y, \omega) = \frac{\mathrm{e}^{-\mathrm{j}\, k_{r,\text{PW}} \cdot x}\, 2\,\pi\, \delta(\omega - \omega_{\text{PW}})}{-\frac{\mathrm{j}}{4}\, H_0^{(2)}\, (k_{r,\text{PW}} \cdot x)}\, 2\,\pi\, \delta(k_y - k_{y,\text{PW}}) \tag{34}$$

and depends on the distance x from the SSD. The sound field is therefore only correctly synthesized at the chosen reference

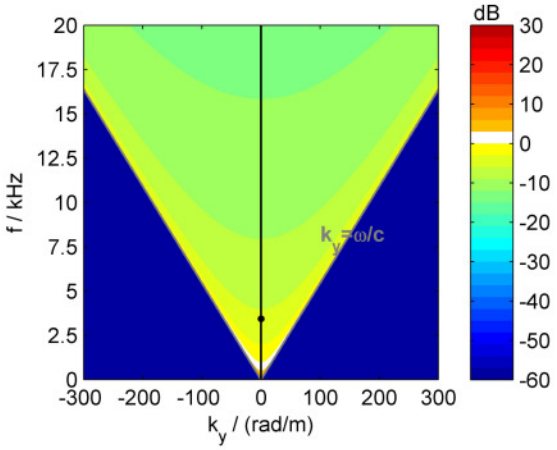

(a) Angular magnitude spectrum of $G_0(k_y, \omega)$. Ideal driving function $D(k_y, \omega)$ for a full-band cylindrical wave into x-direction schematically indicated with a black line, the dot indicates the contribution for $f = 3430$ Hz.

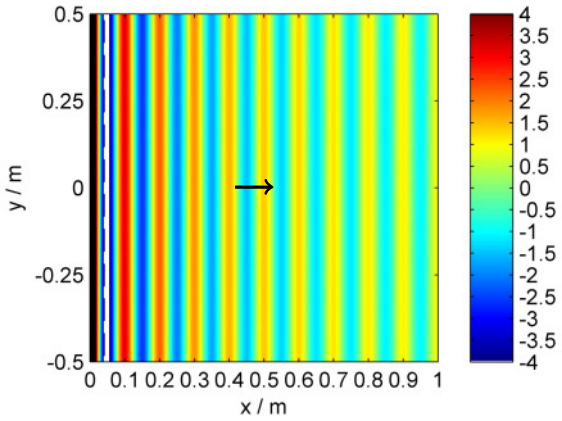

(b) Cylindrical wave into x-direction with $f = 3430\,\text{Hz}$ synthesized by a continuous SSD of infinite length.

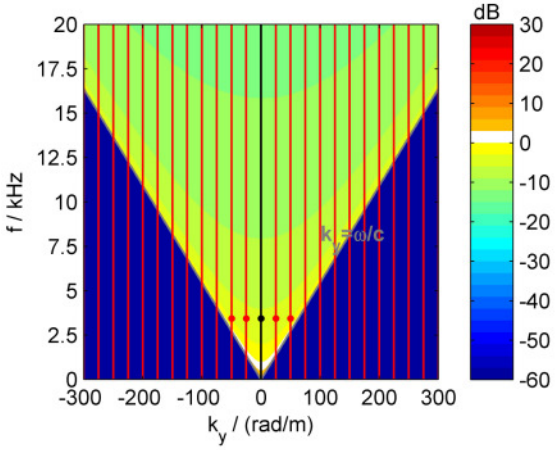

(c) $|G_0(k_y, \omega)|$ and sampled driving function $D_\text{S}(k_y, \omega)$, discretized with $\Delta y \approx 0.25\,\text{m}$. Spectral repetitions indicated in red. The frequency $f = 3430\,\text{Hz}$ is above the spatial Nyquist frequency, propagating aliasing contributions marked by red dots.

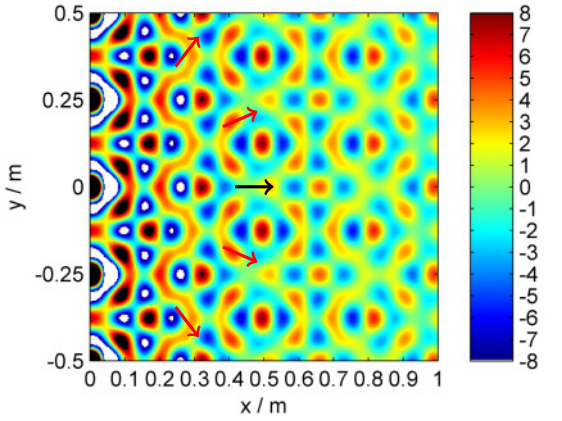

(d) The same intended wave as above, here synthesized by a discretized SSD using $\Delta y \approx 0.25\,\text{m}$. The red arrows show the directions of propagating spatial aliasing components.

Fig. 3: Ideal sound field synthesis by a continuous SSD (top) and with spatial aliasing due to a discretized SSD (bottom). The angular spectra of the driving functions $D(k_y, \omega)$, $D_\text{S}(k_y, \omega)$ and of the farfield Green's function $G_0(k_y, \omega)$ ($x_\text{ref} = 100\,\text{m}$) shown on the left. Magnitude of $G_0(k_y, \omega)$ in dB is normalized to $k_y = 0\,\text{rad/m}$ and $f = 1\,\text{kHz}$ with a 3 dB step colormap. Corresponding wave fields $\Re\{P(\mathbf{x})\}$ in the xy-plane for the frequency $f = 3430$ Hz are depicted on the right side.

line $x = x_\text{ref}$. A spatial inverse Fourier transform (6) of (34) yields [17, (17)]

$$D_\text{2.5D,SDM}(x_\text{ref}, y_0, \omega) = \frac{\exp[-\text{j}\,\frac{\omega_\text{PW}}{c}\,\cos\varphi_\text{PW}\cdot x_\text{ref}]}{-\frac{\text{j}}{4}\,H_0^{(2)}\left(\frac{\omega_\text{PW}}{c}\,\cos\varphi_\text{PW}\cdot x_\text{ref}\right)} \times \exp[-\text{j}\,\frac{\omega_\text{PW}}{c}\,\sin\varphi_\text{PW}\cdot y_0]\;2\,\pi\,\delta(\omega-\omega_\text{PW}). \tag{35}$$

It can be shown that 2.5D SFS does not reproduce a desired plane wave using a linear SSD. The sound field rather exhibits an amplitude decay proportional to $1/\sqrt{x}$ in the farfield which is typical for a cylindrical wave amplitude decay [44, (3.38)], [17, (20)].

We specify (34) towards our special problem of interest: The radiation perpendicular to the SSD within the xy-plane. Therefore $k_{y,\text{PW}} = 0$ is chosen, i.e. $\varphi_\text{PW} = 0$ from which $k_{x,\text{PW}} = \frac{\omega_\text{PW}}{c}$ follows. The adapted driving function's angular

spectrum reads

$$D(x_{\text{ref}}, k_y, \omega) = \frac{\mathrm{e}^{-\mathrm{j}\,\frac{\omega_{\text{PW}}}{c}\cdot x_{\text{ref}}}\, 2\,\pi\,\delta(\omega-\omega_{\text{PW}})}{-\frac{\mathrm{j}}{4}\,H_0^{(2)}\left(\frac{\omega_{\text{PW}}}{c}x_{\text{ref}}\right)}\, 2\,\pi\,\delta(k_y) \quad (36)$$

For $\frac{\omega_{\text{PW}}}{c}\cdot x_{\text{ref}} \gg 1$ the large argument approximation of the Hankel function [45, 10.2.6] leads to the proportionality

$$\left|\frac{1}{-\frac{\mathrm{j}}{4}\,H_0^{(2)}\left(\frac{\omega_{\text{PW}}}{c}x_{\text{ref}}\right)}\right| \propto \left|\sqrt{\frac{\omega_{\text{PW}}}{c}\cdot x_{\text{ref}}}\right|. \quad (37)$$

Hence, the driving function (34) inherently includes a 3 dB/oct. temporal frequencies highpass filter for the case of our interest. For further discussion we omit the compensation filter (37) and the phase shift $\mathrm{e}^{-\mathrm{j}\,\frac{\omega_{\text{PW}}}{c}\cdot x_{\text{ref}}}$ in (36) and restrict the driving function's angular spectrum to

$$D(k_y, \omega) = 2\,\pi\,\delta(k_y)\cdot 2\,\pi\,\delta(\omega-\omega_{\text{PW}}), \quad (38)$$

which yields the driving function

$$D(y_0, \omega) = 1\cdot 2\,\pi\,\delta(\omega-\omega_{\text{PW}}) \quad (39)$$

by inverse spatial Fourier transform. Eq. (39) confirms that an infinite, continuous line source driven with constant volume acceleration produces a cylindrical wave with a 3 dB/oct. lowpass behavior and a 3 dB level drop per distance doubling in the farfield, cf. [24, pg. 12]. In essence the 3 dB/oct. highpass (37) compensates the temporal frequency lowpass characteristics of the line source. In practical LSA applications this is referred to as the coupling filter.

The angular spectrum of the desired full band driving function–we omit the dependence on $2\,\pi\,\delta(\omega-\omega_{\text{PW}})$ from here on–

$$D(k_y, \omega) = 2\,\pi\,\delta(k_y) \quad (40)$$

is depicted in Fig. 3a, together with the farfield Green's function $G_0(x_{\text{ref}}, k_y, \omega)$ (29). For a full audio-bandwidth wavefront into x-direction, $D(k_y, \omega)$ takes the shape of a vertical line. The propagating part of $G_0(k_y, \omega)$ is bounded to the triangular region where $|k_y| \leq |\frac{\omega}{c}|$, this also referred to as the *visible region* of the array. Then, each point coincident with $D(k_y, \omega)$ corresponds to a monochromatic cylindrical wave, as exemplarily shown for a single frequency in Fig. 3b. This plot was realized by using (35) with $\varphi_{\text{PW}} = 0$, $\omega_{\text{PW}} = 2\,\pi\cdot 3430\,\text{rad/s}$ and $x_{\text{ref}} = 1\,\text{m}$ in the discretized version of (23)

$$P(\mathbf{x}, \omega) = \sum_{n\in\mathbb{Z}} D_{\text{2.5D,SDM}}(x_{\text{ref}}, y_{0,n}, \omega)\, G(\|\mathbf{x}-\mathbf{x_{0,n}}\|, \omega)\, \Delta y_0 \quad (41)$$

using a 50 m long SSD, centered at the origin with $\Delta y = 2\,\pi/500\,\text{m}$. Due to the chosen parameters the SSD can be considered as continuous (discretization does not generate spatial aliasing) and infinitely long (negligible truncation artifacts in the plotted region). The wave field exhibits a -3 dB magnitude decay per distance doubling and has a positive unit amplitude along the reference line $x_{\text{ref}} = 1\,\text{m}$ as desired.

Finally, the temporal-frequency lowpass behavior of a line source can be observed in the Green's function's magnitude along the line of $D(k_y, \omega)$ in Fig. 3a.

IV. SFS Signal Processing Framework

The SFS signal processing framework in Fig. 2 was introduced in [15], [19], [30] for WFS. The methods will be applied to our problem of interest in what follows.

A. Spatial Truncation of the Line Soure

Practical arrays are obviously restricted to a finite length. This is realized by truncating the driving function with a spatial window $w(\mathbf{x_0}) \in \mathbb{R}$ in our signal processing model, cf. Fig. 2. With this signal processing step the Rayleigh integral is thus transformed to the Rayleigh-Sommerfeld diffraction integral [47, Ch. 8.11.2], [38, Ch. 6.4]. The synthesized sound field will thus only be correct in the so called Fresnel region in front of the array [48] if either the SSD is enclosed into a rigid wall or –for SSD setups free in space– the length of the SSD is much larger larger than the considered wavelength λ and the wavelength is much smaller than the evaluation distance $\|\mathbf{x}-\mathbf{x_0}\|$. A thorough treatment of possible windowing artifacts in this context (i.e. leakage, near-/farfield characteristics [1]) is beyond the scope of this contribution. Truncation is discussed in detail in [25]. For concise argumentation, we consider only the discretization of the SSD in the remainder of this paper and assume $w(y_0) = 1$.

B. Spatial Discretization of the Line Source

A continuous SSD cannot be realized in practice and is usually implemented as a linear array of discrete loudspeakers. This constitutes a spatial sampling process of the driving function as depicted in Fig. 2 and Fig. 4 (whereby ignoring the truncation w and H_{Pre}, H_{Post} processing stages for the moment). Assuming identical speakers, equidistantly arranged with Δy, ideal sampling is modeled by multiplication with an accordingly spaced Dirac comb. The discretized driving function $D_{\text{S}}(y_0, \omega)$ reads

$$D_{\text{S}}(y_0, \omega) = D(y_0, \omega)\cdot \underbrace{\sum_{\mu=-\infty}^{+\infty} \delta(y_0-\mu\,\Delta y)}_{=:\,\frac{1}{\Delta y}\text{Ш}(\frac{y_0}{\Delta y})}, \quad (42)$$

where the shorthand notation is obtained by dilating a Dirac comb $\text{Ш}(y_0) := \sum_{\mu=-\infty}^{+\infty}\delta(y_0-\mu)$ [49, (11.1)] with unit spacing. The spatial Fourier transform pair for the Dirac combs (42) is known as

$$\underbrace{\sum_{\mu=-\infty}^{+\infty} \delta(y_0-\mu\,\Delta y)}_{=:\,\frac{1}{\Delta y}\text{Ш}(\frac{y_0}{\Delta y})} \circ\!\!-\!\!\bullet \underbrace{\frac{2\,\pi}{\Delta y}\sum_{\mu=-\infty}^{+\infty}\delta\left(k_y-\mu\frac{2\,\pi}{\Delta y}\right)}_{=:\,\text{Ш}(\frac{k_y\,\Delta y}{2\pi})}. \quad (43)$$

With [49, (11.33)]

$$D(y_0, \omega)\cdot\frac{1}{\Delta y}\text{Ш}(\frac{y_0}{\Delta y}) \circ\!\!-\!\!\bullet \frac{1}{2\,\pi}\,D(k_y, \omega) *_{k_y} \text{Ш}(\frac{k_y\,\Delta y}{2\pi}) \quad (44)$$

we obtain the angular spectrum of the ideally sampled driving function

$$D_{\text{S}}(k_y, \omega) = \frac{1}{\Delta y}\sum_{\mu=-\infty}^{+\infty} D(k_y-\mu\,\frac{2\,\pi}{\Delta y}, \omega). \quad (45)$$

For our problem at hand we thus have to deal with the sampled version of (40)

$$D_{\text{S}}(k_y, \omega) = \frac{2\,\pi}{\Delta y}\sum_{\mu=-\infty}^{+\infty}\delta(k_y-\mu\,\frac{2\,\pi}{\Delta y}). \quad (46)$$

In Fig. 3c $D_{\mathrm{S}}(k_y, \omega)$ is schematically indicated for a spatially discretized SSD using a secondary source spacing of $\Delta y \approx 0.25\,\mathrm{m}$ for which the spatial Dirac comb spacing $\Delta k_y = 2\,\pi / \Delta\, y = 25\,\mathrm{rad/m}$ holds. Compared to Fig. 3a the additional repetitions in the angular spectrum stemming from the Dirac comb are clearly indicated. Their coincidences with non-zero values of the Green's function indicate additional propagating contributions in the synthesized sound field. This is commonly called spatial aliasing.

The resulting sound field can be analytically given (cf. [17, Sec. IV.B]), when the angular spectrum

$$P(x, k_y, 0, \omega) = D_{\mathrm{S}}(k_y, \omega) \cdot G_0(x, k_y, 0, \omega) \tag{47}$$

for the considered xy-half-plane undergoes an inverse spatial Fourier transform (6). This yields [17, (37)]

$$P(x, y, 0, \omega) = \frac{1}{\Delta y}\, 2\,\pi\, \delta(\omega - \omega_{\mathrm{CW}}) \times \sum_{\mu=-\infty}^{+\infty} G_0(x, k_y = \mu\, \frac{2\,\pi}{\Delta y}, 0, \omega) \cdot \mathrm{e}^{-\mathrm{j}\,\mu\, \frac{2\,\pi}{\Delta y}\, y}, \tag{48}$$

by inverse spatial Fourier transform and subsequent simplification. For $|\mu\, \Delta k_y| < \frac{\omega}{c}$ only propagating waves are taken into account, which reduces the sum in (48) to finite extent. The exponential term in (48) describes the component along the y-dimension. Note the discrete set of possible wave numbers due to the discrete driving function's angular spectrum. The Green's function's angular spectrum describes the component into radial direction. Both components together describe a cylindrical wave with radiation angle φ_μ. For $\mu = 0$ the intended cylindrical wave perpendicular to the SSD (i.e. into x-direction) is generated. For all other μ that fulfill $|\mu\, \Delta k_y| < \frac{\omega}{c}$ propagating cylindrical waves are synthesized that manifest as spatial aliasing. The radiating angles $\varphi_{\mu \neq 0}$ of the spatial aliasing wave fronts are derived with $\sin \varphi_{\mu \neq 0} = (k_{y, \mu \neq 0}) / \frac{\omega}{c}$ and are strongly dependent of the temporal angular frequency ω. For frequencies smaller than

$$f < \frac{c}{\Delta y\, (1 + |\sin \varphi_{\mathrm{PW}}|)}, \tag{49}$$

no propagating spatial aliasing components will be synthesized, cf. [17, (38)]. For our problem at hand $\varphi_{\mathrm{PW}} = 0$, (49) reduces to

$$f < \frac{c}{\Delta y} \quad \leftrightarrow \quad \Delta y < \lambda \tag{50}$$

denoting the wavelength λ in m, cf. [1, sec. II.3.a]. Thus, for $\Delta y < \lambda$ the Green's function generates a propagating wave only for $\mu = 0$ and no spatial aliasing occurs. Note that this criterion is different from that found in [3, sec. 3.1] for a discretized linear array of *finite* length ($\Delta y < \lambda/2$, WST #2). In [1, II.3.a.] an equivalent derivation is given and a sound field, that is corrupted by spatial aliasing, was named "chaotic", which is a deterministic phenomenon due to (48).

Thus, for a spatially discretized SSD (here $\Delta y \approx 0.25\,\mathrm{m}$), a propagating sound field for $f = 3430\,\mathrm{Hz}$ is synthesized which consists of the desired cylindrical wave into x-direction plus four weighted spectral repetitions at $\mu = \pm 1, \pm 2$ in (46) due to $|\mu\, \Delta k_y| < \frac{\omega}{c}$. The radiating angles of the additional cylindrical waves are derived to $\varphi_{\mu = \pm 1,2} = \pm 23.4°, \pm 52.7°$. The resulting sound field is depicted in Fig. 3d. This plot was realized by using (35) with $\varphi_{\mathrm{PW}} = 0$, $\omega_{\mathrm{PW}} = 2\,\pi \cdot 3430\,\mathrm{rad/s}$ and $x_{\mathrm{ref}} = 1\,\mathrm{m}$ in (41) with a 50 m long SSD, centered at the origin with $\Delta y = 2\,\pi / 25\,\mathrm{m}$. The originally intended wave (cf. Fig. 3b) is corrupted due to destructive and constructive interferences with the additional waves. The chosen SSD discretization does not allow the reproduction of a homogeneous wave at this frequency. It is important realizing that the sound field remains corrupted over the full space when performing SFS with an infinite SSD. This is in contrast to finite length SSDs, where a spatial aliasing free region exists in far distances to the SSD, cf. [25].

Spatial aliasing should obviously be avoided for uniform sound reinforcement in the listening area. We therefore need a methodology to suppress the spatial repetitions in the driving function's angular spectrum (46). This will be elaborated in the next sections.

C. Pre-/Postfilter for the Ideal Sampling Model

In classical baseband sampling theory the prefilter $H_{\mathrm{Pre}}(y_0, \omega)$ and the postfilter $H_{\mathrm{Post}}(y_0, \omega)$ in Fig. 2 and Fig. 4 are usually understood as the anti-aliasing and the reconstruction filter respectively, both with ideal spatial lowpass characteristics. Before sampling the driving function, $H_{\mathrm{Pre}}(k_y, \omega)$ must ideally suppress all contributions for $|k_y| > \pi / \Delta x$ (i.e. above the Nyquist frequency) ensuring a correctly sampled baseband. Subsequently, the ideal postfilter $H_{\mathrm{Post}}(k_y, \omega)$ removes all spectral repetitions in $D_s(k_y, \omega)$ for correct baseband reconstruction. Artifacts due to a non-ideal prefilter have been termed *aliasing error* or *pre-aliasing*, those due to the postfiltering stage *reconstruction error* or *post-aliasing*, cf. [50]. In SFS literature the different aliasing types are typically not strictly separated in terminology and *spatial aliasing* is used to subsume all artifacts. In the context of SDM theoretical spatial postfiltering schemes were discussed in [22], [51].

In most practical SFS applications and radiation synthesis approaches however, explicit spatial pre- and postfiltering is omitted in the discussion (i.e. $H_{\mathrm{Pre}}(k_y, \omega) = H_{\mathrm{Post}}(k_y, \omega) = 1$). For our radiation synthesis problem at hand, dropping the prefilter is well justified: the continuous driving function $D(k_y, \omega)$ in (40) is already spatially band-limited and pre-aliasing cannot occur.

Omitting the postfilter on the other hand is not recommended: Using (47) with (29) and (46), the sound field $P(x, k_y, 0, \omega)$ is synthesized as a product of the two functions $D_S(k_y, \omega)$ and $G_0(x, k_y, 0, \omega)$, which both exhibit infinite spatial bandwidth. This results in post-aliasing as illustrated in Fig. 3d. Therefore we aim for a spatial lowpass postfilter. The corresponding sampling model in the angular spectrum domain is shown in the block diagram in Fig. 4.

With (47) and (46) we deduce, cf. [22, (36)]

$$P(x, k_y, 0, \omega) = \overbrace{D_S(k_y, \omega) \cdot \underbrace{H_{\mathrm{Post}}(k_y, \omega)}_{\text{loudspeaker as spatial lowpass}}}^{\text{ideal sampling}} \cdot G_0(x, k_y, 0, \omega) \tag{51}$$

and may define

$$G'(x, k_y, 0, \omega) = H_{\mathrm{Post}}(k_y, \omega) \cdot G_0(x, k_y, 0, \omega), \tag{52}$$

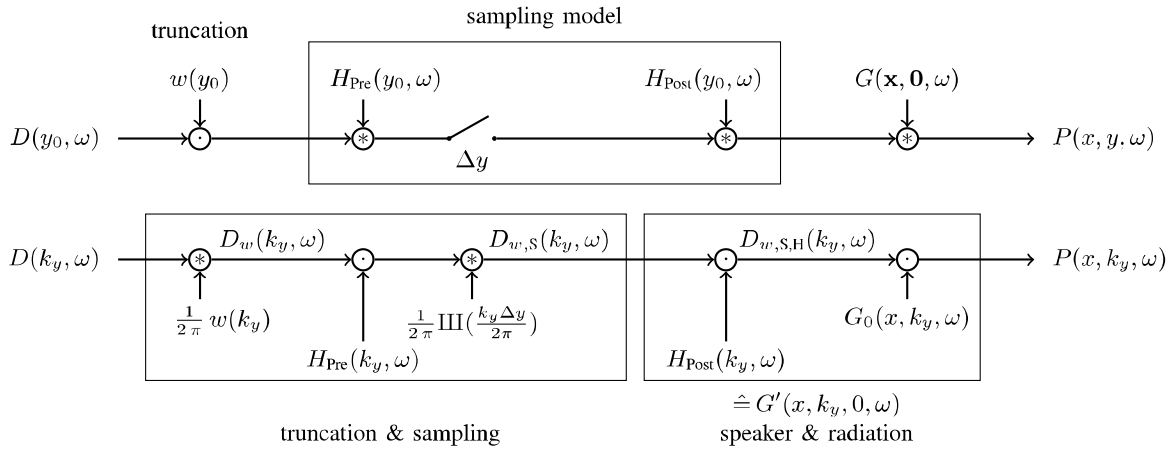

Fig. 4: The single layer potential for a linear, spatially discretized and truncated SSD in time-frequency domain (top) and angular spectrum domain (bottom).

which we term *Green's-like function*[3] . The postfilter is split from the sampling stage and merged with the Green's function. This allows us to model an ideally sampled driving function and take loudspeaker farfield directivities into account, cf. (10). In practice the used loudspeakers exhibit a finite spatial bandwidth and thus operate as a (non-ideal) reconstruction filter. This method was also used in [18], [19], [22]. In [51, sec. 3.1] theoretical spatial lowpass secondary sources were discussed and denoted $G_{\text{anti-alias}}$.

We proceed with the derivation of Green's-like functions for baffled piston models (as also done in [1]), which will serve for further examination of our problem.

V. Piston Green's-like Functions

The farfield radiation characteristics of a plane baffled piston is derived from the Rayleigh integral's farfield approximation [26, (26.4)], [43, (2.84)]

$$P_{\text{Far}}(\mathbf{x},\omega) = 2\,\mathrm{j}\,\omega\,\rho_0\,G(\|\mathbf{x}-\mathbf{x_0}\|,\omega)\times \iint_{-\infty}^{+\infty} V_n(\mathbf{x_0},\omega)\,\mathrm{e}^{+\mathrm{j}(k_y\,y_0+k_z\,z_0)}\,\mathrm{d}y_0\,\mathrm{d}z_0 \tag{53}$$

for which $\frac{\omega}{c}\,\|\mathbf{x}-\mathbf{x_0}\| \gg 1$. The piston is here located in the yz-plane, thus $\mathbf{x_0} = (0, y_0, z_0)$. The evaluation points are denoted by $\mathbf{x} = (x > 0, y, z)$. The nominal atmospheric density is denoted by ρ_0 in kg/m^3. We use the piston's normal velocity temporal spectrum $V_n(\mathbf{x_0},\omega)$ into x-direction. With (7) the integral in (53) is identified as the two-dimensional spatial Fourier transform $V_n(y_0,z_0,\omega) \circ\!\!-\!\!\bullet\; V(k_y,k_z,\omega)$ and therefore

$$P_{\text{Far}}(\mathbf{x},\omega) = 2\,\mathrm{j}\,\omega\,\rho_0\,G(\|\mathbf{x}-\mathbf{x_0}\|,\omega)\cdot V(k_y,k_z,\omega). \tag{54}$$

We extend (54) with the complex source strength temporal spectrum, sometimes referred to as the volume flow $Q(\omega)$ [27, pg. 175], [26, ch. 18.3]

$$P_{\text{Far}}(\mathbf{x}) = 2\,Q(\omega)\,\mathrm{j}\,\omega\,\rho_0\,G(\|\mathbf{x}-\mathbf{x_0}\|,\omega)\,\underbrace{\frac{V(k_y,k_z,\omega)}{Q(\omega)}}_{H(k_y,k_z,\omega)} \tag{55}$$

and define the dimensionless directivity function $H(k_y,k_z,\omega)$ [26, (26.7)]. The freefield Green's function is usually interpreted as a velocity potential Φ stemming from a unit source, so (55) is rewritten accordingly:

$$\Phi_{\text{Far}}(\mathbf{x},\omega) = 2\,Q(\omega)\,G(\|\mathbf{x}-\mathbf{x_0}\|,\omega)\,H(k_y,k_z,\omega) \tag{56}$$

using $P(\mathbf{x},\omega) = \mathrm{j}\,\omega\,\varrho_0\,\Phi(\mathbf{x},\omega)$ [26, ch. 13.8]. For our half-space problem at hand, the volume flow is normalized to $Q = 1/2\,(\text{m}^3/\text{s})/\text{Hz}$ to be consistent with the unit volume flow of the freefield (full space) Green's function. The Green's-like function for our 2.5D SFS problem – we only consider k_y– then reads

$$\begin{aligned}\Phi_{\text{Far,unitQ}}(\mathbf{x},\omega) =& G'(\|\mathbf{x}-\mathbf{x_0}\|,\omega)\\ =& G(\|\mathbf{x}-\mathbf{x_0}\|,\omega)\cdot H(k_y,\omega)\end{aligned} \tag{57}$$

and the spatial Fourier transform with respect to y yields

$$G'(x,k_y,0,\omega) = G_0(x,k_y,0,\omega)\cdot H(k_y,\omega) \tag{58}$$

using (29). We recognize $H(k_y,\omega) = H_{\text{Post}}(k_y,\omega)$ ((58) vs. (52)), that we previously used to interpret the product of the freefield Green's function and a spatial postfilter for the reconstruction process within the SFS signal processing model. Recall that $k_y = \frac{\omega}{c}\,\sin\varphi$, so $H_{\text{Post}}(k_y,\omega)$ could be interpreted as a function of φ as well, which is a familiar representation of loudspeaker directivity patterns, here for the vertical orientation. Note that evanescent waves are not considered since the postfilter model holds only under farfield assumptions. As a formal consequence, we define $H_{\text{Post}}(k_y,\omega) = 0$ for $|k_y| > \frac{\omega}{c}$.

A single spherical monopole located at $\mathbf{x_0} = \mathbf{0}$ exhibits a postfilter $H_{\text{Monopole}}(k_y,\omega) = 1$.

A baffled circular piston with radius r_0 ($r_0^2 = y_0^2 + z_0^2$) located in the yz-plane, centered around the origin and driven

[3]Note that this is not a Green's function by strict definition, rather a particular solution of the wave equation with a different inhomogeneity $\neq \delta(\mathbf{x}-\mathbf{x_0})$. We have chosen the term to stress its role of a propagator into space. Informally speaking, G' does for a loudspeaker modeled with its farfield directivity what G_0 does for monopoles.

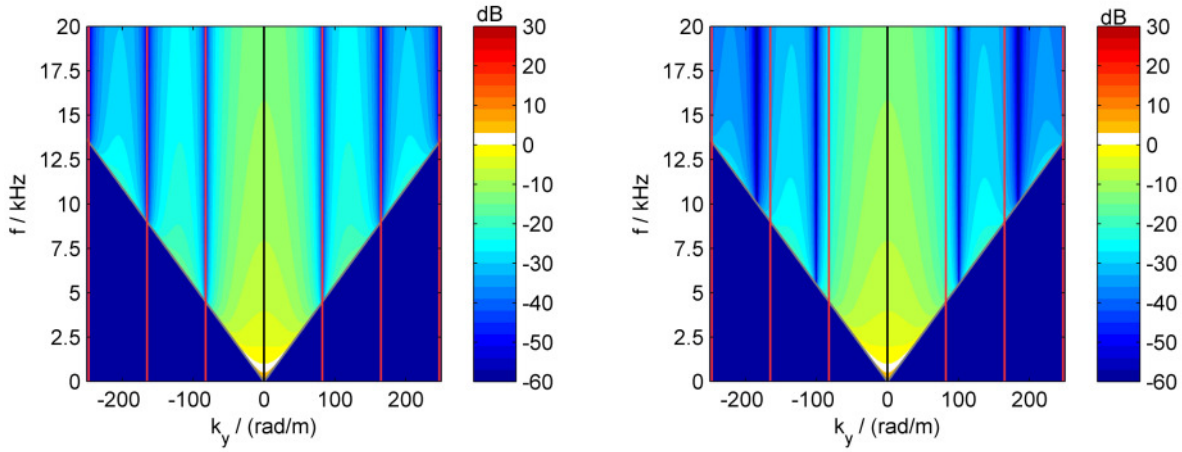

(a) $|G'_{\text{Rect}}(k_y,\omega)|$ for a line piston with length $l = 3" = 0.0762\,\text{m}$. $D_S(k_y,\omega)$ for an SSD discretization $\Delta y = l$ is indicated.

(b) $|G'_{\text{Circ}}(k_y,\omega)|$ for a circular piston with diameter $d = 2\,r_0 = 3" = 0.0762\,\text{m}$. $D_S(k_y,\omega)$ for an SSD discretization $\Delta y = 2\,r_0$ is indicated.

Fig. 5: Comparison of postfilters for a line and circular piston of same dimensions. Magnitude of farfield $G'_{\text{circ}}(k_y,\omega)$ in dB is normalized to $k_y = 0\,\text{rad/m}$ and $f = 1\,\text{kHz}$ with a 3 dB step colormap.

with constant velocity is described by the postfilter [26, (26.42)], [27, (7.4.17)]

$$H_{\text{Circ}}(k_y,\omega) = \frac{2\,J_1(k_y\,r_0)}{k_y\,r_0} = \frac{2\,J_1(\frac{\omega}{c}\,\sin\varphi\,r_0)}{\frac{\omega}{c}\,\sin\varphi\,r_0}, \tag{59}$$

where $J_1(\cdot)$ denotes the cylindrical Bessel function of 1st kind of 1st order [45, (10.2.2)]. Note that for negative k_y [45, (10.11.1)] is valid.

A baffled linear piston of length l and infinitesimal width located at $|y_0| \leq l/2$ with constant velocity is characterized by the postfilter [26, (26.44)], [27, (7.3.3)]

$$H_{\text{Rect}}(k_y,\omega) = \frac{\sin\left(k_y\,\frac{l}{2}\right)}{k_y\,\frac{l}{2}} = \frac{\sin\left(\frac{\omega}{c}\,\sin\varphi\,\frac{l}{2}\right)}{\frac{\omega}{c}\,\sin\varphi\,\frac{l}{2}}. \tag{60}$$

In Fig. 5 the Green's-like angular spectra for a line piston and a circular piston of same dimension ($l = 3"$ and $r_0 = 3"/2$ respectively) are depicted. For increasing k_y magnitude decay indicates spatial lowpass characteristics.

VI. Infinite and Discretized Line Source Array

We now discuss LSA design criteria for spatial-aliasing-free sound field reproduction. Recall our problem at hand using (46) and (51) for a desired spatial-aliasing-free cylindrical wave into x-direction, i.e. $k_x = \frac{\omega}{c}$, $k_y = 0$, $k_z = 0$.

Table I indicates the frequency range for discretized SSDs. We recognize that the spacing between secondary sources must not exceed a few mm to reproduce a full band spatial-aliasing-free sound field, cf. [3, pg. 918]. This was not considered a feasible approach in the past, although commercial LSA designs[4] with $\Delta y = 21\,\text{mm}$ exist meanwhile.

Instead of, an LSA element is designed with electrodynamic loudspeakers for the low and mid frequencies and employs waveguides for the high frequencies $> 1 - 2\,\text{kHz}$.

[4] e.g. Martin Audio OmniLine®

A. Reproduction with Circular Pistons

We model an electrodynamic loudspeaker for $\lambda > r_0$ with a circular piston using the reconstruction filter (59). Circular pistons with radius $r_0 = 15"/2$ and $r_0 = 6.5"/2$ as indicated in Tab. I are discussed due to their practical usage for LSA element designs. In Fig. 6a, 6b the Green's-like functions $G'_{\text{circ}}(k_x)$ are depicted in the angular spectrum domain. They exhibit the directivity pattern of (59) compared to that of a spherical monopole in Fig. 3a. The Green's-like function will be triggered by the spectral repetitions of the sampled driving function's angular spectrum $D_S(k_y,\omega)$ (46). Due to the spatial lowpass characteristics, repetitions are attenuated. This produces a sound field with less spatial aliasing. In order to avoid it completely, ideal band limitation in the temporal frequency domain has to be applied to the driving function, cf. [51, sec. 3.1.2]. In our ideal examples this would require a temporal frequency lowpass with cut frequencies at f_{LP} =900 Hz and f_{LP} =2078 Hz respectively. For multi-way loudspeaker designs bandpass crossovers are employed. In real applications the crossover lowpass frequency is much lower than the critical anti-aliasing frequency due to electro-acoustical concerns. We therefore conclude that perfect spatial-aliasing suppression is uncritical for the low and mid audio frequencies.

$\Delta y = 15" = 0.381$ m	$f_{\text{no aliasing}} < 900\,\text{Hz}$
$\Delta y = 6.5" = 0.1651\,\text{m}$	$f_{\text{no aliasing}} < 2078\,\text{Hz}$
$\Delta y = 3" = 0.0762\,\text{m}$	$f_{\text{no aliasing}} < 4501\text{Hz}$
$\Delta y = 1" = 0.0254\,\text{m}$	$f_{\text{no aliasing}} < 13504\text{Hz}$

TABLE I: Anti-aliasing condition (50) for a discretized, infinite SSD that should reproduce a cylindrical wave front perpendicular to the SSD. Δy indicates the theoretically minimum possible spacing between adjacent, non-overlapping circular pistons with radius $r_0 = \Delta y/2$.

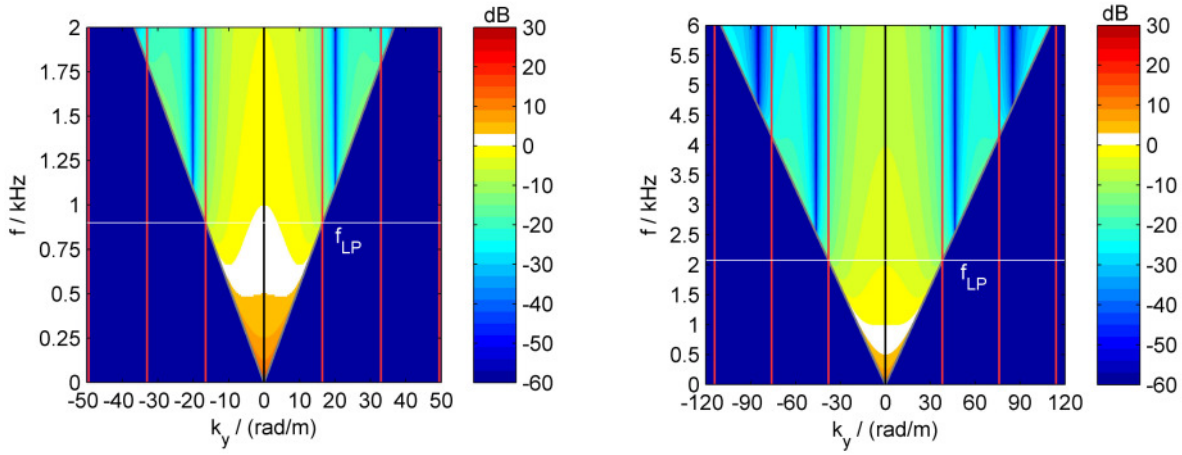

(a) 15” circular piston

(b) 6.5” circular piston

Fig. 6: $|G'_{\text{circ}}(k_y,\omega)|$ for two circular pistons with radius $r_0 = 0.1905\,\text{m}$ (left) and $r_0 = 0.08255\,\text{m}$ (right). $|G'_{\text{circ}}(k_y,\omega)|$ exhibits spatial lowpass characteristics. The sampled driving function' angular spectrum $D_S(k_y,\omega)$ with $\Delta y = 2\,r_0 \leftrightarrow \Delta k_y = \frac{2\,\pi}{\Delta y}$ is indicated by vertical lines. Magnitude of $G'_{\text{circ}}(k_y,\omega)$ in dB is normalized to $k_y = 0\,\text{rad/m}$ and $f = 1\,\text{kHz}$ with a 3 dB step colormap. Note the different scaling of the temporal frequency axis f and wave number axis k_y.

B. Reproduction with an Ideal Waveguide

Since the required small distances between the secondary sources for high frequencies were not feasible in the past, waveguides were introduced in the literature [2, Fig. 11]. Recall that we want to realize the driving function $D(y_0,\omega) = 1$ (39). From [1, I.3.] and [3, Fig. 6] we deduce that a waveguide can be modeled as a line piston of length l. The resulting driving function using waveguides is piece-wise constant with amplitudes $D(y_0,\omega) \in \{0,1\}$. This is illustrated in Fig. 7 and represents the reconstructed driving function $D_{\text{S,Rect}}(y_0,\omega)$. A similar visualization was used in [3, Fig. 6] to motivate waveguide modeling. We proceed to derive $D_{\text{S,Rect}}(y_0,\omega)$ analytically. The postfilter $H_{\text{Post}}(y_0,\omega) = H_{\text{Rect}}(y_0,\omega)$ is expressed as the rect-function, cf. [49, (9.19)]

$$H_{\text{Rect}}(y_0,\omega) = \text{rect}\left(\frac{y_0}{l}\right) = \begin{cases} 1 & \text{for } |y_0| \leq \frac{l}{2} \\ 0 & \text{else} \end{cases} \quad . \tag{61}$$

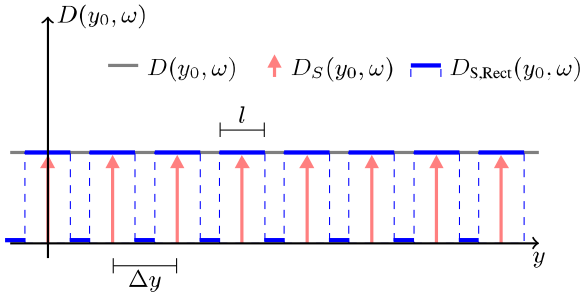

Fig. 7: Spatial discretization and reconstruction: continuous driving function $D(y_0)$, ideally sampled driving function $D_{\text{S}}(y_0)$ and reconstructed driving function $D_{\text{S,Rect}}(y_0)$ with the rect-function used as the postfilter.

and is convolved with the ideally sampled driving function $D_S(y_0,\omega)$ (42), cf. Fig. 4. This can be given as

$$D_{\text{S,Rect}}(y_0,\omega) = \left[1 \cdot \sum_{\mu=-\infty}^{+\infty} \delta(y_0 - \mu\,\Delta y)\right] *_y \text{rect}\left(\frac{y_0}{l}\right). \tag{62}$$

The Dirac comb stemming from $D_S(y_0,\omega)$ (Fig. 7, red) is smeared by the convolution with the rect-function yielding $D_{\text{S,Rect}}(y_0,\omega)$ (Fig. 7, blue). By splitting the postfilter from the sampling process and merging it with the Green's function (52), we see that the Green's-like function becomes an ideal, baffled, linear piston with length l and constant potential, instead of an ideal monopole.

From Fig. 7 we graphically deduce that the driving function $D(y_0,\omega) = D_{\text{S,Rect}}(y_0,\omega) = 1$ is perfectly reconstructed for $l = \Delta y$ as intended for spatial-aliasing-free sound field reproduction. This is proven within the angular spectrum domain: With the spatial Fourier transform (7) of (61) [49, (9.24)]

$$H_{\text{Rect}}(k_y,\omega) = l \cdot \frac{\sin\left(\frac{k_y\,l}{2}\right)}{\frac{k_y\,l}{2}} = l \cdot \text{sinc}\left(\frac{k_y\,l}{2}\right) \tag{63}$$

we re-identify the proposed postfilter (60). Note the normalization mismatch by l that stems from our chosen definition of a unit source Green's-like function, which is independent of the piston's length, cf. (56). Inserting (46) and (63) into $D_{\text{S,Rect}}(k_y,\omega) = D_S(k_y,\omega) \cdot H_{\text{Rect}}(k_y,\omega)$ of (51) we obtain

$$D_{\text{S,Rect}}(k_y,\omega) = \left[\frac{1}{\Delta y} \sum_{\mu=-\infty}^{+\infty} 2\,\pi\,\delta(k_y - \mu\,\frac{2\,\pi}{\Delta y})\right] l\,\frac{\sin\left(\frac{k_y\,l}{2}\right)}{\frac{k_y\,l}{2}}. \tag{64}$$

Hence for $l = \Delta y$ follows

$$D_{\text{S,Rect}}(k_y, \omega) = \sum_{\mu=-\infty}^{+\infty} 2\,\pi\,\delta(k_y - \mu\,\frac{2\,\pi}{\Delta y}) \cdot \frac{\sin\left(\frac{k_y\,\Delta y}{2}\right)}{\frac{k_y\,\Delta y}{2}}. \tag{65}$$

The impulses w.r.t. μ in the Dirac comb with spacing $\Delta k_y = 2\,\pi/\Delta y = 2\,\pi/l$ are weighted by the sinc-function. The individual contributions read

$$D_{\text{S,Rect}}(k_y, \omega)_\mu = 2\,\pi\,\delta(k_y - \mu\,\frac{2\,\pi}{\Delta y}) \frac{\sin\left(\frac{\mu\,\frac{2\,\pi}{\Delta y}\,\Delta y}{2}\right)}{\frac{\mu\,\frac{2\,\pi}{\Delta y}\,\Delta y}{2}}, \tag{66}$$

$$D_{\text{S,Rect}}(k_y, \omega)_\mu = 2\,\pi\,\delta(k_y - \mu\,\frac{2\,\pi}{\Delta y}) \frac{\sin(\mu\,\pi)}{\mu\,\pi}. \tag{67}$$

For $\mu = 0$ we get (40)

$$D_{\text{S,Rect}}(k_y, \omega)_{\mu=0} = 2\,\pi\,\delta(k_y) = D(k_y, \omega) \tag{68}$$

and for $\mu \neq 0$ we get due to the zeros of the sine function

$$D_{\text{S,Rect}}(k_y, \omega)_{\mu\neq 0} = 0. \tag{69}$$

This proves perfect reconstruction

$$D_{\text{S,Rect}}(k_y, \omega) = \begin{cases} D(k_y, \omega) = 2\,\pi\,\delta(k_y) & \text{if } \mu = 0 \\ 0 & \text{otherwise} \end{cases}. \tag{70}$$

In Fig. 5a the Green's-like function $G'_{\text{Rect}}(k_y, \omega)$ and $D_S(k_y, \omega)$ (46) are depicted for a line piston with length $l = \Delta y = 0.0762\,\text{m}$. The intended driving function $D(k_y, \omega) = 2\,\pi\,\delta(k_y)$ is perfectly reconstructed and no spatial aliasing occurs. This is due to the complete suppression of the driving function's energy for $\mu \neq 0$ by the zeros of the sinc-term in the Green's-like function (60). Note that the zeros of the sinc-function are equidistantly spaced with $\Delta k_y = 2\,\pi/\Delta y$ which does not hold for the Bessel function $J_1(\cdot)$ that was used for circular pistons.

We conclude that the usage of a line piston for this special case (uniformly driven array and $\Delta y = l$) is superior compared to a circular piston for high frequencies: In the ideal case all spatial aliasing energy is suppressed. This is not achievable with circular pistons. However, for $\Delta y > l$ (this case is depicted in Fig. 7, cf. [3, fig. 6]) the repetitions exhibit smaller steps Δk_y compared to Fig. 5a. The spectral repetitions no longer coincide with the zeros of the Green's-like function and the quality of the spatial lowpass determines the suppression of spatial aliasing. The comparison of a line and circular with same dimension in Fig. 5 reveals an improved spatial lowpass characteristics of the circular piston.

We can furthermore deduce, that it is obviously preferable to use rather small Δy (i.e. large Δk_y) and thereby small pistons. Thus, in the ideal case no spectral repetitions would enter the visible region $|k_y| < \frac{\omega}{c}$ of the SSD, which allows radiation synthesis with a high degree of freedom within the propagating part of (29). This is useful for LSA designs, that aim at electronical beamsteering and -forming methods, rather than using geometry shaping of an uniform driven LSA, since the spatial aliasing energy is triggered at very high temporal frequencies, and thus ideally leaving the audio frequency band uncorrupted from spatial aliasing. This implies that ideally no additional postfilter is required and only the Green's functions acts as the reconstruction interpolator of the sampled driving function. For very small Δy, and thus very small chosen r_0 and l, the postfilters of the circular and line piston become less directive, as desired for this approach. In essence this was confirmed in the simulations performed in [14]. It was proven that a high driving granularity of the LSA–and thus using small pistons–offers a higher degree of freedom for finding driving functions to synthesize an optimized sound field[5]. Further discussions on the postfilter characteristics for LSA applications can be found [25]. This paper also revisits the WST criterion 1 [3, sec. 3.2], that was derived for line piston driven LSAs. This criterion introduced the Active Radiation Factor (ARF) for an arbitrarily chosen tolerable aliasing contribution. For a large number of LSA elements an ARF $= l/\Delta y \geq 0.82$ was defined in order that aliasing contributions are at least 13.5 dB lower than that of the desired wave front, which is consistent with the discussions here for an infinite LSA. We proceed with a comparison of our line piston modeling with a measurement of a commercially available waveguide.

C. Reproduction with a Real Waveguide

This subsection examines the spatial lowpass characteristics of a commercial LSA element. An equiangular 2°-spherical balloon dataset of impulse responses from the single loudspeaker box was measured in the far- and freefield, cf. (54). The vertical isobars, i.e. the plane wave propagation angles $-\pi/2 \leq \varphi \leq +\pi/2$ for $\vartheta = \pi/2$ were extracted, smoothed in magnitude by 1/6 oct. and mapped to $k_y = \frac{\omega}{c}\sin\varphi$. All frequency responses were normalized by the temporal spectrum of $k_y = 0$, therefore linearizing the spectrum on the main axis $\varphi = 0$. This yields the reconstruction filter $H_{\text{Post}}(k_y, \omega) = H_{\text{Waveguide}}(k_y, \omega)$. Subsequently a 3 dB/oct. lowpass was applied to all spectra to obtain the Green's-like function $G'_{\text{Waveguide}}(k_y, \omega)$, cf. (58). This allows for direct comparison of the theoretical line piston Green's-like function (58)&(60) with the measured one. For the interesting frequencies >1 kHz the behavior of the measured waveguide can be considered as baffled due to the loudspeaker box dimension/wavelength ratio. Because of the nonlinear mapping $k_y = \frac{\omega}{c}\sin\varphi$ the balloon dataset is not considered optimal for this examination. We rather suggest a measurement along a line and a subsequent spatial Fourier transform (7) to obtain an equidistant k_x-resolution, instead of an equiangular resolution, cf. [52], [53].

We assume a sampling distance $\Delta y = 0.36\,\text{m}$ due to the LSA element height, and an ARF=1. In Fig. 8a the Green's-like function $G'_{\text{Rect}}(k_y, \omega)$ of an ideal waveguide corresponding to sec. VI-B is depicted for $\Delta y = l$. In Fig. 8b the measured Green's-like function $G'_{\text{Waveguide}}(k_y, \omega)$ is shown for comparison. The model and measurement are in good agreement.

An additional analysis with a common vertical isobar plot is conducted, which requires a remapping of the data in Fig. 8b. The isobar plot is depicted in Fig. 9 up to 20 kHz. We normalized all spectra to get a linearized, flat spectrum on its main axis (i.e. for $k_y = 0$, $\varphi = 0$). The spatial-aliasing energy contributions are then given as absolute attenuation values within the surface plot. The black horizontal line again represents the intended driving function. The repetitions

[5] A commercial LSA design that employs this approach is e.g. the EAW Anya™ system.

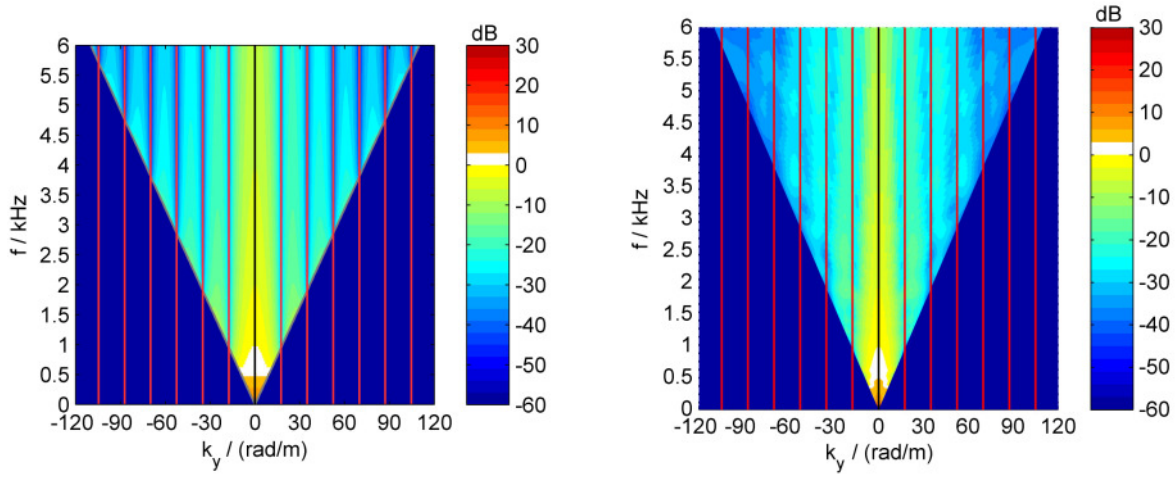

(a) Ideal line piston $|G'_{\text{Rect}}(k_y, \omega)|$.

(b) Measured waveguide $|G'_{\text{Waveguide}}(k_y, \omega)|$.

Fig. 8: $|G'(k_y, \omega)|$ and $D_S(k_y, \omega)$ with $\Delta y = l = 0.36$ m.

$|\mu| \leq 4$, $\mu \neq 0$ are indicated with red curves. We recognize that the driving function repetitions are coincident with the zeros of the Green's-like function and thus will be suppressed. This confirms our modeling in sec. VI-B and good spatial lowpass characteristics of the measured waveguide. Above 11 kHz the attenuation slightly becomes less than 10 dB for the first repetition $|\mu| = 1$. For $|\mu| > 4$ the Green's-like function attenuates the driving function repetitions > 20 dB. It is worth to note that Fig. 9 does not visualize the directivity of a whole LSA but rather that of a single waveguide in its farfield.

VII. Conclusion

Based on sound field synthesis fundamentals, the sound field radiation from a discretized, infinite, linear and uniformly driven source was described. The radiation synthesis problem for a line source array application was formulated for a continuous secondary source distribution. Spatially sampling of a suitable driving function models discrete loudspeaker positions. This sampling process was then discussed in the angular spectrum domain and the importance of a suitable postfilter was emphasized. In practice the used loudspeakers act as spatial reconstruction filters. By introducing loudspeaker directivities, the WST criteria for required spatial-aliasing-free sound field reproduction with a line source array were confirmed. We conclude that spatial-aliasing-free sound fields for high frequencies should be synthesized with line source arrays that employ waveguides with an ideal active radiation factor of one. Based on the discussions it is furthermore suggested to choose a rather fine driving granularity, i.e. small, individually driven pistons. This approach would displace the spatial aliasing problem to higher temporal frequencies and therefore a higher degree of freedom with regard to electronic beamforming is achieved. This would allow improved performance of finding driving functions in recently developed numerical optimization schemes [10]–[14]. A real waveguide measurement was presented that complies with the criteria and is in good agreement with the proposed modeling. An alternative interpretation of commonly used vertical isobar plots of loudspeaker directivities was introduced.

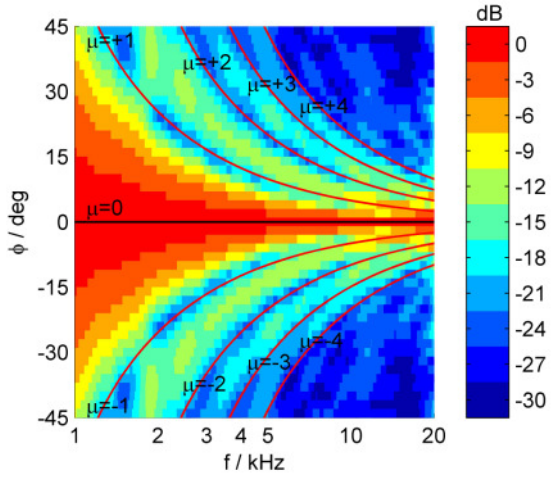

Fig. 9: Measured waveguide $|G'_{\text{Waveguide}}(k_y, \omega)|$ from Fig. 8b as an isobar plot. Magnitude is normalized to $\varphi = 0$. Hence the absolute attenuation values of the spatial aliasing energy contributions are presented. The spectral repetitions $|\mu| \leq 4$, $\mu \neq 0$ due to the discretized SSD are shown as red curves.

VIII. Acknowledgement

The authors would like to thank Anselm Goertz for providing the loudspeaker balloon dataset of the examined line source array loudspeaker box.

References

[1] Heil, C.; Urban, M. (1992): "Sound fields radiated by multiple sound sources arrays." In: *Proc. of 92nd Audio Eng. Soc. Convention, Vienna*, #3269.

[2] Urban, M.; Heil, C.; Baumann, P. (2001): "Wavefront Sculpture Technology." In: *Proc. of 111th Audio Eng. Soc. Convention, New York*, #5488.

[3] Urban, M.; Heil, C.; Baumann, P. (2003): "Wavefront Sculpture Technology." In: *J. Audio Eng. Soc.*, **51**(10):912–932.

[4] Ureda, M.S. (2004): "Analysis of loudspeaker line arrays." In: *J. Audio Eng. Soc.*, **52**(5):467–495.

[5] Jacob, K.D.; Birkle, T.K. (1990): "Prediction of the full-space directivity characteristics of loudspeaker arrays." In: *J. Audio Eng. Soc.*, **38**(4):250–259.

[6] Gunness, D.W.; Hoy, W.R. (1999): "Improved loudspeaker array modeling." In: *Proc. of 107th Audio Eng. Soc. Convention, New York*, #5020.

[7] Ahnert, W.; Baird, J.; Feistel, S.; Meyer, P. (2000): "Accurate electroacoustic prediction utilizing the complex frequency response of far-field polar measurements." In: *Proc. of 108th Audio Eng. Soc. Convention, Paris*, #5129.

[8] Baird, J.; Meyer, P.; Meyer, J. (2001): "Far-field loudspeaker interaction: Accuracy in theory and practice." In: *Proc. of 110th Audio Eng. Soc. Convention, Amsterdam*, #5309.

[9] Feistel, S.; Thompson, A.; Ahnert, W. (2009): "Methods and limitations of line source simulation." In: *J. Audio Eng. Soc.*, **57**(6):379–402.

[10] van Beuningen, G.W.J.; Start, E.W. (2000): "Optimizing directivity properties of DSP controlled loudspeaker arrays." In: *Proc. of the Institute of Acoustics*, 22(6).

[11] Thompson, A. (2009): "Improved methods for controlling touring loudspeaker arrays." In: *Proc. of 127th Audio Eng. Soc. Convention, New York*, #7828.

[12] Thompson, A.; Baird, J.; Webb, B. (2011): "Numerically optimised touring loudspeaker arrays - Practical applications." In: *Proc. of 131st Audio Eng. Soc. Convention, New York*, #8511.

[13] Feistel, S.; Sempf, M.; Köhler, K.; Schmalle, H. (2013): "Adapting loudspeaker array radiation to the venue using numerical optimization of FIR filters." In: *Proc. of 135th Audio Eng. Soc. Convention, New York*, #8937.

[14] Thompson, A.; Luzarraga, J. (2013): "Drive granularity for straight and curved loudspeaker arrays." In: *Proc. of the Institute of Acoustics*, 35(2).

[15] Start, E.W.; Valstar, V.G.; de Vries, D. (1995): "Application of spatial bandwidth reduction in wave field synthesis." In: *Proc. of the 98th Audio Eng. Soc. Convention, Paris*, #3972.

[16] Spors, S.; Rabenstein, R.; Ahrens, J. (2008): "The theory of Wave Field Synthesis revisited." In: *Proc. of the 124th Audio Eng. Soc. Convention, Amsterdam*, #7358.

[17] Ahrens, J.; Spors, S. (2010): "Sound field reproduction using planar and linear arrays of loudspeakers." In: *IEEE Trans. Audio Speech Language Process.*, **18**(8):2038–2050.

[18] de Vries, D. (1996): "Sound reinforcement by wavefield synthesis: Adaptation of the synthesis operator to the loudspeaker directivity characteristics." In: *J. Audio Eng. Soc.*, **44**(12):1120–1131.

[19] Verheijen, E. (1997): *Sound Reproduction by Wave Field Synthesis*. Ph.D. thesis, Delft University of Technology.

[20] Ahrens, J.; Spors, S. (2010): "An analytical approach to 2.5D sound field reproduction employing linear distributions of non-omnidirectional loudspeakers." In: *Proc. of 35th Intl. Conference on Acoustics, Speech and Signal Processing (IEEE 35th ICASSP), Dallas*, 105–108.

[21] Koyama, S.; Furuya, K.; Hiwasaki, Y.; Haneda, Y. (2012): "Sound field reproduction method in spatio-temporal frequency domain considering directivity of loudspeakers." In: *Proc. of the 132nd Audio Eng. Soc. Convention, Budapest*, #8664.

[22] Firtha, G.; Fiala, P. (2012): "Prefiltering the wave field synthesis operators - anti-aliasing and source directivity." In: *Intl. Conference on Noise and Vibration Engineering (ISMA 2012), Leuven, Belgium*, 3121 – 3136.

[23] Hahn, N. (2013): "Sound field simulation using extrapolated impulse responses." In: *Proc. of the 52nd Audio Eng. Soc. Intl. Conference on Sound Field Control, Guildford*.

[24] Lipshitz, S.P.; Vanderkooy, J. (1986): "The acoustic radiation of line sources of finite length." In: *Proc. of 81st Audio Eng. Soc. Convention, Los Angeles*, #2417.

[25] Schultz, F.; Rettberg, T.; Spors, S. (2014): "On spatial-aliasing-free sound field reproduction using finite length line source arrays." In: *Proc. of the 137th Audio Eng. Soc. Convention, Los Angeles*, #9098.

[26] Skudrzyk, E. (1971): *The Foundations of Acoustics*. New York, Wien: Springer.

[27] Kinsler, L.E.; Frey, A.R.; Coppens, A.B.; Sanders, J.V. (2000): *Fundamentals of Acoustics*. Hoboken: Wiley, 4. ed.

[28] Meyer, P.; Schwenke, R. (2003): "Comparison of the directional point source model and BEM model for arrayed loudspeakers." In: *Proc. of the Institute of Acoustics*, 25(4).

[29] Schultz, F.; Spors, S. (2014): "Comparing approaches to the spherical and planar single layer potentials for interior sound field synthesis." In: *Acta Acust United Ac*, **100**(6):900–911.

[30] Start, E.W. (1997): *Direct Sound Enhancement by Wave Field Synthesis*. Ph.D. thesis, Delft University of Technology.

[31] Verheijen, E. (2010): *Sound Reproduction by Wave Field Synthesis*. Ph.D. thesis, Delft University of Technology.

[32] Spors, S. (2006): "Spatial aliasing artifacts produced by linear loudspeaker arrays used for wave field synthesis." In: *Proc. of the 2nd Intl. Symposium on Control, Communications and Signal Processing (EURASIP 2nd ISCCSP), Marrakech*.

[33] Spors, S.; Rabenstein, R. (2006): "Spatial aliasing artifacts produced by linear and circular loudspeaker arrays used for wave field synthesis." In: *Proc. of the 120th Audio Eng. Soc. Convention, Paris*, #6711.

[34] Spors, S.; Ahrens, J. (2009): "Spatial sampling artifacts of wave field synthesis for the reproduction of virtual point sources." In: *Proc. of the 126th Audio Eng. Soc. Convention, Munich*, #7744.

[35] Spors, S.; Ahrens, J. (2010): "Analysis and improvement of pre-equalization in 2.5-dimensional Wave Field Synthesis." In: *Proc. of the 128th Audio Eng. Soc. Convention, London*, #8121.

[36] Ahrens, J.; Spors, S. (2012): "Applying the Ambisonics approach to planar and linear distributions of secondary sources and combinations thereof." In: *Acta Acust United Ac*, **98**(1):28–36.

[37] Fazi, F.M.; Nelson, P.A. (2013): "Sound field reproduction as an equivalent acoustical scattering problem." In: *J. Acoust. Soc. Am.*, **134**(5):3721–3729.

[38] Nieto-Vesperinas, M. (2006): *Scattering And Diffraction in Physical Optics*. Singapore: World Scientific, 2. ed.

[39] Berkhout, A.J. (1988): "A holographic approach to acoustic control." In: *J. Audio Eng. Soc.*, **36**(12):977–995.

[40] Berkhout, A.J.; de Vries, D.; Vogel, P. (1993): "Acoustic control by Wave Field Synthesis." In: *J. Acoust. Soc. Am.*, **93**(5):2764–2778.

[41] Vogel, P. (1993): *Application of Wave Field Synthesis*. Ph.D. thesis, Delft University of Technology.

[42] Ahrens, J.; Spors, S. (2008): "Reproduction of a plane-wave sound field using planar and linear arrays of loudspeakers." In: *Proc. of 3rd Intl. Symposium on Communications, Control and Signal Processing (IEEE 3rd ISCCSP), Malta*, 1486–1491.

[43] Williams, E.G. (1999): *Fourier Acoustics. Sound Radiation and Nearfield Acoustic Holography*. London, San Diego: Academic Press, 1. ed.

[44] Ahrens, J. (2012): *Analytic Methods of Sound Field Synthesis*. Heidelberg: Springer, 1. ed.

[45] Olver, F.W.J.; Lozier, D.W.; Boisvert, R.F.; Clark, C.W. (2010): *NIST Handbook of Mathematical Functions*. Cambridge University Press, 1. ed.

[46] Start, E.W. (1996): "Application of curved arrays in Wave Field Synthesis." In: *Proc. of the 100th Audio Eng. Soc. Convention, Copenhagen*, #4143.

[47] Born, M.; Wolf, E. (2006): *Principles of optics*. Cambridge: Cambridge University Press, 7th (expanded), 4th printing ed.

[48] Schultz, F.; Spors, S. (2014): "On the frequency response variation of sound field synthesis using linear arrays." In: *Fortschritte der Akustik: Tagungsband d. 40. DAGA, Oldenburg*, 592–593.

[49] Girod, B.; Rabenstein, R.; Stenger, A. (2001): *Signals and Systems*. Chichester: Wiley, 1. ed.

[50] Mitchell, D.P.; Netravali, A.N. (1988): "Reconstruction filters in computer graphics." In: *Computer Graphics*, **22**(4):221–228.

[51] Ahrens, J.; Spors, S. (2010): "On the anti-aliasing loudspeaker for sound field synthesis employing linear and circular distributions of

secondary sources." In: *Proc. of the 129th Audio Eng. Soc. Convention, San Francisco*, #8246.

[52] Pueo, B.; Lpez, J.J.; Escolano, J.; Bleda, S. (2007): "Analysis of multiactuator panels in the space-time wavenumber domain." In: *J. Audio Eng. Soc.*, **55**(12):1092–1106.

[53] Koyama, S.; Furuya, K.; Hiwasaki, Y.; Haneda, Y. (2011): "Sound field recording and reproduction using transform filter designed in spatio-temporal frequency domain." In: *Proc. of the 131st Audio Eng. Soc. Convention, New York*, #8544.

UPDATES

2014-10-06 initial version